AGU PUBLICATIONS

JGR

Journal of Geophysical Research: Space Physics

RESEARCH ARTICLE
10.1002/2016JA023371

Special Section:
Major Results From the MAVEN Mission to Mars

MAVEN measured oxygen and hydrogen pickup ions: Probing the Martian exosphere and neutral escape

A. Rahmati[1], D. E. Larson[1], T. E. Cravens[2], R. J. Lillis[1], J. S. Halekas[3], J. P. McFadden[1], P. A. Dunn[1], D. L. Mitchell[1], E. M. B. Thiemann[4], F. G. Eparvier[4], G. A. DiBraccio[5], J. R. Espley[5], C. Mazelle[6], and B. M. Jakosky[4]

[1]Space Sciences Laboratory, University of California, Berkeley, California, USA, [2]Department of Physics and Astronomy, University of Kansas, Lawrence, Kansas, USA, [3]Department of Physics and Astronomy, University of Iowa, Iowa City, Iowa, USA, [4]Laboratory for Atmospheric and Space Physics, University of Colorado Boulder, Boulder, Colorado, USA, [5]NASA Goddard Space Flight Center, Greenbelt, Maryland, USA, [6]IRAP/CNRS, Toulouse, France

Key Points:
- Model-data comparisons of MAVEN SEP, SWIA, and STATIC measured oxygen and hydrogen pickup ions are presented
- Three case studies demonstrate how pickup ion model-data comparisons can constrain Mars exospheric neutral densities
- Factor of 10 change with Mars season in the hydrogen exosphere is observed, whereas the oxygen exosphere remained steadier

Correspondence to:
A. Rahmati,
rahmati@ssl.berkeley.edu

Citation:
Rahmati, A., et al. (2017), MAVEN measured oxygen and hydrogen pickup ions: Probing the Martian exosphere and neutral escape, *J. Geophys. Res. Space Physics*, *122*, doi:10.1002/2016JA023371.

Received 20 AUG 2016
Accepted 3 JAN 2017
Accepted article online 7 JAN 2017

©2017. American Geophysical Union. All Rights Reserved.

Abstract Soon after the MAVEN (Mars Atmosphere and Volatile EvolutioN) spacecraft started orbiting Mars, the SEP (Solar Energetic Particle), SWIA (Solar Wind Ion Analyzer), and STATIC (Supra-Thermal and Thermal Ion Composition) instruments on board the spacecraft detected planetary pickup ions. SEP can measure energetic (>60 keV) oxygen pickup ions, the source of which is the extended hot oxygen exosphere of Mars. Model results show that these pickup ions originate from tens of Martian radii upstream of Mars and are energized by the solar wind motional electric field as they gyrate back toward Mars. SWIA and STATIC can detect both pickup oxygen and pickup hydrogen with energies below ~30 keV and created closer to Mars. In this study, data from the SEP, SWIA, and STATIC instruments containing pickup ion signatures are provided and model-data comparisons are shown. During the times when MAVEN is outside the Martian bow shock and in the upstream undisturbed solar wind, the solar wind velocity measured by SWIA and the solar wind (or interplanetary) magnetic field measured by the MAG (magnetometer) instrument can be used to model pickup oxygen and hydrogen fluxes. By comparing measured pickup ion fluxes with model results, the Martian thermal hydrogen and hot oxygen neutral densities can be probed outside the bow shock, providing a helpful tool in constraining estimates of neutral oxygen and hydrogen escape rates. Our analysis reveals an order of magnitude density change with Mars season in the hydrogen exosphere, whereas the hot oxygen exosphere was found to remain steadier.

1. Introduction

One of the main goals of the MAVEN (Mars Atmosphere and Volatile EvolutioN) mission to Mars is to characterize atmospheric escape [*Bougher et al.*, 2014; *Jakosky et al.*, 2015a; *Lillis et al.*, 2015], which occurs in the form of neutrals and ions. In the present epoch, neutral escape on Mars mainly takes place in the form of photochemical (nonthermal) escape of atomic oxygen [*Chassefière and Leblanc*, 2004] and Jeans (thermal) escape of atomic hydrogen [*Chamberlain and Hunten*, 1987]. Both processes populate an exosphere that extends beyond the Martian bow shock and directly interacts with the solar wind [e.g., *Jakosky et al.*, 1994, 2015c; *Brecht and Ledvina*, 2006, 2010; *Lundin et al.*, 2013; *Ramstad et al.*, 2015; *Brain et al.*, 2010, 2015; *Dong et al.*, 2015a, 2015b; *Ma et al.*, 2015]. The oxygen exosphere at Mars is populated by hot oxygen atoms that are created photochemically in the ionosphere via the dissociative recombination of O_2^+ molecules with electrons [e.g., *Nagy and Cravens*, 1988]. Some of the newly created neutral oxygen atoms in this reaction gain energies above the escape energy at Mars and can escape from the planet, given favorable initial directions and sufficiently few and/or small-angle collisions with background neutrals [e.g., *Ip*, 1988].

Martian exospheric oxygen densities and escape rates have, in the past, been modeled with different degrees of complexity and for different solar wind, solar cycle, and seasonal conditions [*Nagy and Cravens*, 1988; *Ip*, 1988, 1990; *Kim et al.*, 1998; *Kaneda et al.*, 2009; *Valeille et al.*, 2009a, 2009b, 2010; *Yagi et al.*, 2012; *Fox and Hać*, 2009, 2010, 2014; *Rahmati et al.*, 2014; *Lee et al.*, 2015a, 2015b]. These models, however, vary by as much as 2 orders of magnitude in estimates of neutral oxygen escape from Mars with photochemical escape rates ranging from a few times $10^{24}\,s^{-1}$ to a few times $10^{26}\,s^{-1}$. New models of oxygen escape will utilize MAVEN data to give improved escape estimates; and while the stream of new data from MAVEN has exponentially expanded our knowledge of the Mars upper atmosphere, neutral escape calculations using in situ MAVEN observations are complicated by a dynamic thermosphere and ionosphere environment with significant spatial and temporal variabilities in parameters needed for escape calculations [*Bougher et al.*, 2015; *Benna*

et al., 2015; *Mahaffy et al*., 2015b; *Andrews et al*., 2015; *Jain et al*., 2015; *Sakai et al*., 2015, 2016; *Ergun et al*., 2015; *Lillis et al*., 2017, *Bougher et al*., 2017]. At the same time, in situ detection of the escaping neutrals proves impractical due to the very low density of the oxygen exosphere at altitudes where escape is dominating [*Rahmati et al*., 2014].

The first successful attempt in remote sensing of the hot oxygen component present in the Martian exosphere was through spectroscopic observations of the oxygen 130.4 nm triplet during Rosetta's flyby of Mars in February 2007 [*Feldman et al*., 2011]. Since MAVEN's arrival at Mars, the IUVS (Imaging Ultra-Violet Spectrograph) instrument [*McClintock et al*., 2015] onboard MAVEN has also taken spectroscopic observations of Mars' upper atmosphere and has found a hot component in the oxygen exosphere with reliable 130.4 nm measurements extending in altitude to just above one Mars radius (1 R_M = 3400 km) [*Deighan et al*., 2015]. Hot oxygen simulation results by *Rahmati et al*. [2014] indicate that the escaping portion of the hot oxygen exosphere becomes dominant at distances greater than ~10 R_M, and that below this altitude the Martian exosphere is mainly populated with gravitationally bound oxygen atoms. *Cravens et al*. [2002] proposed a method by which energetic oxygen pickup ion measurements made by the energetic particle detector on the Phobos-2 spacecraft were used to place constraints on the density of the Mars oxygen exosphere at altitudes extending to several R_M. The same method was adapted by *Rahmati et al*. [2014] showing that the SEP (Solar Energetic Particle) instrument on MAVEN would also be able to detect oxygen pickup ions that are created in the far distant exosphere of Mars and energized by the solar wind motional electric field to energies above ~60 keV, making them detectable by SEP. *Rahmati et al*. [2015] confirmed that SEP indeed detects pickup O^+ originating from several R_M upstream of Mars, giving access to neutral oxygen densities at altitudes never probed before.

The hydrogen exosphere at Mars is populated by thermal hydrogen atoms; the ultraviolet spectrometers on board the Mariner 6 and 7 spacecraft were the first to detect the Lyman α emission from this extended hydrogen exosphere [*Anderson and Hord*, 1971; *Barth et al*., 1971]. Similar measurements were followed by Mariner 9 [*Barth et al*., 1972; *Anderson*, 1974], and also the Mars 2 and 3 spacecraft [*Dostovalov and Chuvakhin*, 1973]. The Lyman α emission from the hydrogen exosphere of Mars has also been derived from background measurements of the neutral particle detector of the ASPERA-3 (Analyzer of Space Plasmas and Energetic Atoms) instrument on Mars Express [*Galli et al*., 2006] and measured by the three more recent ultraviolet spectrometers, namely, SPICAM (Spectroscopy for Investigation of Characteristics of the Atmosphere of Mars) on Mars Express [*Chaufray et al*., 2008], Alice on Rosetta [*Feldman et al*., 2011], and IUVS on MAVEN [*Chaffin et al*., 2015]. The Lyman α emission from the Martian hydrogen corona has also been observed by the ACS/SBC (Advanced Camera for Surveys/Solar Blind Channel) on board the Hubble Space Telescope [*Clarke et al*., 2014]. The ASPERA (Automatic Space Plasma Experiment with Rotating Analyzer) instrument on the Phobos-2 spacecraft was the first to detect hydrogen pickup ions associated with the neutral hydrogen exosphere of Mars, and *Barabash et al*. [1991] used those measurements to put constraints on density profiles of the Martian hydrogen exosphere. Pickup protons were later measured again by the ASPERA-3 Ion Mass Analyzer on the Mars Express spacecraft [*Dubinin et al*., 2006], reaffirming the observations of Phobos-2.

By modeling the trajectories of pickup ions and comparing them with measurements of MAVEN ion analyzers, a link can be established between pickup ion fluxes and their source neutral densities. In this paper, we provide details about the pickup ion model used to simulate trajectories of oxygen and hydrogen pickup ions outside the Martian bow shock in the solar wind and show comparisons of model results with the SEP, SWIA (Solar Wind Ion Analyzer), and STATIC (Supra-Thermal and Thermal Ion Composition) measured pickup ions. We demonstrate that pickup O^+ measurements using SEP, SWIA, and STATIC can constrain neutral oxygen exospheric densities over a broad range of altitudes, ranging from one R_M to tens of R_M. SWIA and STATIC model-data comparisons for pickup H^+ are also provided and used to place constraints on hydrogen exosphere densities at distances up to a few R_M. The neutral densities constructed by using the pickup ion technique presented in this paper will help in constraining neutral escape rates at Mars. Preliminary estimates of neutral oxygen escape will be provided by comparing the results from the pickup ion model and escape rate calculations of *Rahmati et al*. [2014].

2. Pickup Ion Model

Ionization of neutral species within the exosphere of a planet or in the coma of a comet exposes the newly created ions to the electromagnetic fields in the solar wind. The ions are then said to be "picked up" by the

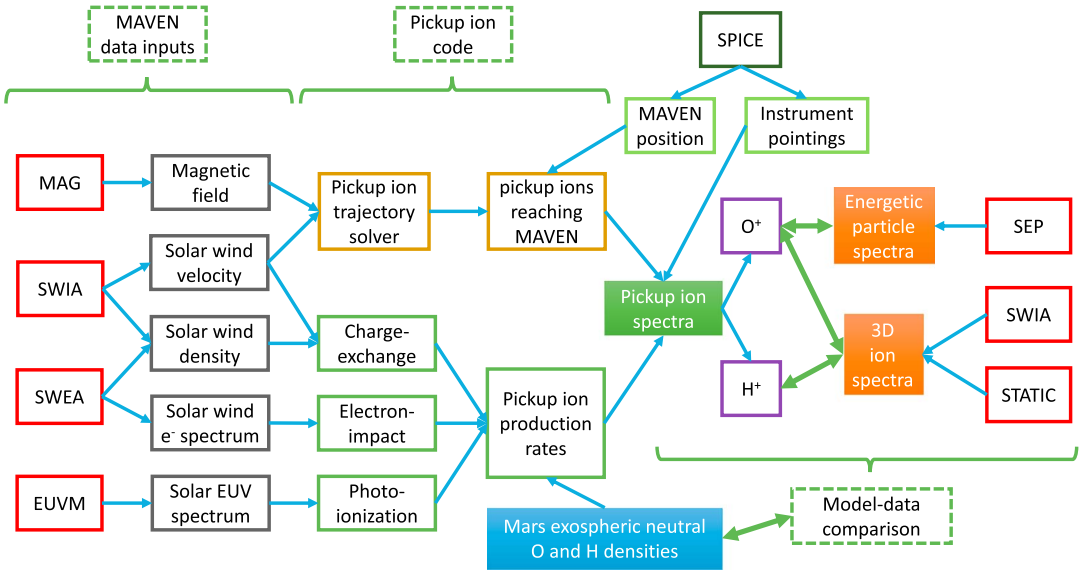

Figure 1. Different working parts of the pickup ion code used in this study. Data from the MAVEN MAG, SWIA, SWEA, and EUVM instruments are used in calculating pickup ion spectra seen by the SEP, SWIA, and STATIC instruments. Model-data comparisons help in constraining the Mars exospheric neutral densities and the associated neutral escape rates.

solar wind motional electric field and start to gyrate about the magnetic field in cycloid motion [e.g., *Cravens*, 2004]. As pickup ions are energized by the solar wind motional electric field, they become detectable by spacecraft instruments [e.g., *Cravens et al.*, 2002; *Dubinin et al.*, 2006; *Jarvinen and Kallio*, 2014; *Goldstein et al.*, 2015]. Many test particle models have simulated pickup ions at Mars for different upstream conditions, ranging from typical solar wind conditions [e.g., *Luhmann*, 1990; *Luhmann and Schwingenschuh*, 1990; *Luhmann and Kozyra*, 1991; *Kallio and Koskinen*, 1999; *Fang et al.*, 2008; *Curry et al.*, 2013, 2014; *Wang et al.*, 2015] to extreme solar wind conditions [*Fang et al.*, 2013; *Curry et al.*, 2015; *Jakosky et al.*, 2015b], and also during the passage of Comet Siding Spring by Mars, which occurred on 19 October 2015 [*Gronoff et al.*, 2014; *Wang et al.*, 2016].

The pickup ion code used in this study is essentially a simplified test particle model that was developed at the University of Kansas and is thoroughly discussed in *Rahmati* [2016]. The same code was previously used by *Rahmati et al.* [2015] to model fluxes of energetic oxygen pickup ions measured by MAVEN SEP. Figure 1 shows a flow diagram representing the order of steps taken in our pickup ion simulation, starting from MAVEN data inputs that feed into the pickup ion code and ending with model-data comparisons. Data from multiple MAVEN instruments are required to model the pickup ions measured by SEP, SWIA, and STATIC. The three components of the interplanetary magnetic field (IMF) as well as the solar wind velocity vectors are needed in calculating the trajectories of pickup ions. The IMF is measured by the MAVEN MAG (magnetometer) instrument at a 32 vectors per second cadence [*Connerney et al.*, 2015a, 2015b]. The solar wind velocity is measured by SWIA at a 4 s cadence [*Halekas et al.*, 2015a]. The pickup ion code downsamples the input data to a lower cadence, typically between 16 and 64 s, depending on output time resolution and calculation speed requirements. The position of MAVEN and its instrument orientations are retrieved by using SPICE kernels [*Acton*, 1996], and the trajectories of pickup ions that reach MAVEN are solved analytically by the pickup ion code.

In calculating the ionization frequencies of pickup ions, three ionization processes are included, i.e., photoionization [*Angel and Samson*, 1988], proton charge exchange [*Fite et al.*, 1960; *Stebbings et al.*, 1964], and electron impact ionization [*Cravens et al.*, 1987]. Photoionization frequencies are calculated by using the solar EUV (extreme ultraviolet) spectrum constructed by the Flare Irradiance Spectral Model (FISM) [*Chamberlin et al.*, 2007], which takes as input, measurements of the EUV Monitor (EUVM) instrument [*Eparvier et al.*, 2015] on MAVEN as a proxy to constrain the solar photon spectrum from 0 nm to 190 nm at daily or minute cadences [*Thiemann et al.*, 2017]. The charge exchange frequency between solar wind protons and exospheric neutral oxygen or hydrogen atoms is calculated by using the solar wind flux measured by SWIA. The electron impact

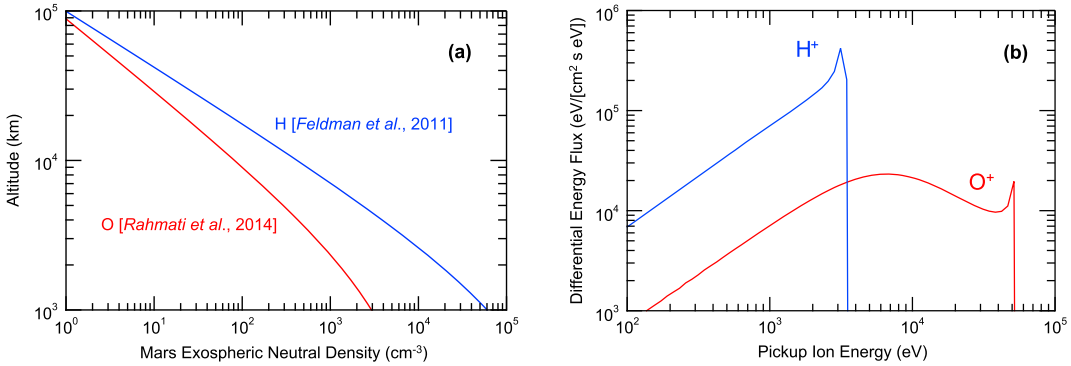

Figure 2. (a) Exospheric altitude profiles of neutral oxygen and hydrogen densities used in the pickup ion model and later adjusted according to pickup ion model-data comparisons. (b) Angle-integrated differential energy fluxes of hydrogen and oxygen pickup ions calculated by the pickup ion code assuming a solar wind velocity of 400 km/s, a magnetic field perpendicular to the solar wind with a strength of 3 nT, and ionization frequencies for both oxygen and hydrogen equal to 3×10^{-7} s^{-1}, with the observation point located at a subsolar altitude of 5000 km.

ionization frequency is calculated by using suprathermal electron flux measurements by the SWEA (Solar Wind Electron Analyzer) instrument on MAVEN [*Mitchell et al*., 2016].

Once ionization frequencies are in hand, pickup ion production rates can be calculated given some knowledge of exospheric neutral density profiles. For atomic oxygen, the exospheric density profile used in the code is taken from the study by *Rahmati et al*. [2014], who modeled the hot oxygen exosphere by using the combination of a hot oxygen two-stream transport and the Liouville theorem. As *Cravens et al*. [2017] discuss, elastic cross sections play a key role in determining hot oxygen exospheric densities and escape rates, but the cross sections are currently uncertain. For atomic hydrogen, the exospheric density profile is taken from *Feldman et al*. [2011], which was derived from the Lyman β measurements of the Alice instrument on the Rosetta spacecraft during Rosetta's flyby of Mars in February 2007. For comparison, both exospheric density profiles are depicted in Figure 2a.

Pickup ion fluxes measured by MAVEN outside the bow shock are proportional to pickup ion production rates, and therefore, to the neutral densities of exospheric oxygen and hydrogen. Thus, comparing measured fluxes with modeled fluxes allows us to constrain the density of neutrals far upstream of Mars. Figure 2b shows typical energy fluxes of pickup ions upstream of the Martian bow shock, calculated by using the density profiles shown in Figure 2a. For this simulation, a solar wind velocity of 400 km/s in the antisunward direction and a magnetic field perpendicular to the solar wind velocity with a strength of 3 nT were assumed. The ionization frequencies for both oxygen and hydrogen were set to 3×10^{-7} s^{-1}. These values correspond to typical solar, solar wind, and IMF conditions. The observation point for this simulation was located at a subsolar altitude of 5000 km, which is just outside the Martian bow shock.

During time periods when part of MAVEN's precessing orbit is located outside the bow shock and in the upstream solar wind, it is possible to use the measured upstream drivers in the pickup ion code and compare the model results with the SEP, SWIA, and STATIC measurements. On their cycloid motion back toward Mars, pickup ions may undergo reflection from the bow shock. The reflected pickup ions are not, however, modeled in our pickup ion code, because the code solves trajectories of pickup ions using MAVEN measured solar wind fields assuming that pickup ions are only traveling outside the bow shock. The reflected pickup ions exhibit different velocity and energy characteristics from pristine solar wind pickup ions [*Dubinin et al*., 2006; *Yamauchi et al*., 2012; *Yamauchi et al*., 2015a; *Frahm et al*., 2016; *Masunaga et al*., 2016, 2017] and are not included in our analysis.

The SEP instrument's ability to detect energetic oxygen pickup ions was discussed in *Rahmati et al*. [2014], and initial model-data comparisons were provided in *Rahmati et al*. [2015]. SWIA and STATIC can detect both pickup O^+ and pickup H^+. SEP, SWIA, and STATIC are briefly described in the following section; more detail about each instrument can be found in their respective description papers [*Larson et al*., 2015; *Halekas et al*., 2015a; *McFadden et al*., 2015].

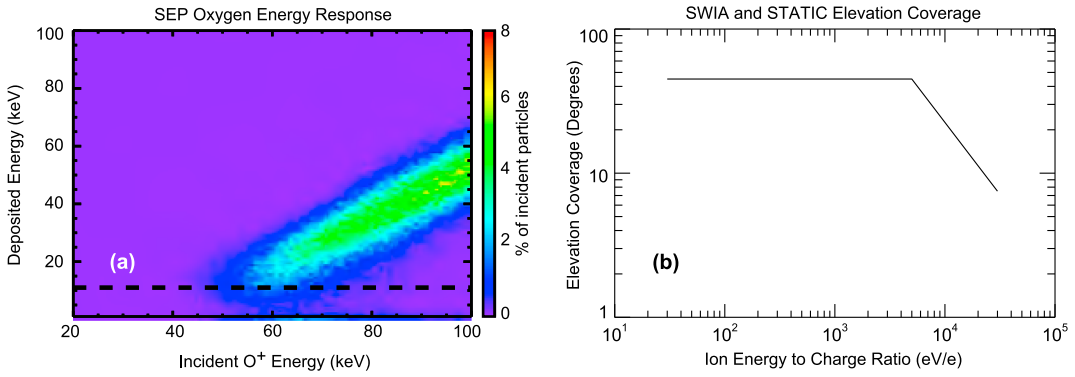

Figure 3. (a) Energy response of SEP to incident oxygen ions. SEP's electronic noise threshold is 11 keV and is marked by the dashed line. Oxygen ions with energies above ~60 keV trigger counts in SEP. (b) Dependence of the SWIA and STATIC's deflection angle (elevation) coverage on the energy of the measured ions. Below 5 keV, the elevation coverage is ±45°. Above 5 keV, the elevation coverage drops proportional to the energy and reaches ±7° at 30 keV.

3. MAVEN SEP, SWIA, and STATIC

MAVEN SEP [*Larson et al*., 2015] is a pair of dual, double-ended solid state telescopes that measures energetic electrons and ions. SEP is also able to detect oxygen pickup ions, the source of which is the extended hot oxygen exosphere of Mars. Each SEP aperture has a rectangular 31° × 42° opening. SEP's energy response to incident oxygen ions is shown in Figure 3a. The horizontal dashed line in Figure 3a marks the electronic noise threshold of SEP, which is 11 keV. Oxygen pickup ions above 60 keV are detectable by SEP; therefore, SEP can only detect pickup O^+ during periods of high solar wind speed [*Rahmati et al*., 2014, 2015]. Since SEP-detected oxygen pickup ions originate in the far upstream exosphere of Mars, they can serve as a diagnostic for neutral oxygen densities in the distant exosphere. Therefore, the flux of SEP-measured oxygen pickup ions provides a direct probe of the exospheric neutral densities tens of R_M upstream of Mars, where neutral oxygen atoms are mainly escaping. Pickup O^+ fluxes measured by SEP can thus be used to place constraints on hot oxygen photochemical escape rates. SEP is blind to pickup H^+, as the maximum pickup hydrogen energy in the solar wind (which is 4 times the solar wind proton energy of ~1 keV) is well below the low-energy threshold for detection of hydrogen in SEP (which is ~20 keV).

The SWIA [*Halekas et al*., 2015a] and STATIC [*McFadden et al*., 2015] instruments on MAVEN are electrostatic ion analyzers that are able to measure energy and angle distributions of both oxygen and hydrogen pickup ions at Mars. SWIA can measure ions with an energy-to-charge ratio of 25 eV to 25 keV, in 96 logarithmically spaced energy bins, using 24 anodes that cover 360° in instrument azimuth. In order for SWIA to characterize the solar wind with sufficient angular resolution, 10 of the 24 anodes (10 fine anodes) cover the 45° in azimuth facing the Sun when the spacecraft is in nominal Sun-pointing mode. Therefore, the azimuthal resolution in the sunward direction is 4.5°. The rest of the anodes (14 coarse anodes) cover the remainder of the azimuth (315°), giving each of them an angular coverage of 22.5°. SWIA does not have the capability to discriminate ions based on mass. STATIC, on the other hand, includes a time of flight (TOF) capability to resolve ion masses with a resolution of $\Delta M/M = 25\%$. Each mass channel of STATIC is less susceptible to background noise compared to SWIA's background level, due to the anticoincidence capability of the TOF system [*McFadden et al*., 2015]. The TOF system, however, reduces STATIC's geometric factor compared to that of SWIA, making it less suitable for high time resolution study of lower flux pickup ions. STATIC measures ion distributions in 64 logarithmically spaced energy steps that, depending on the instrument mode, can range from 0.1 eV to 30 keV. Both SWIA and STATIC use electrostatic deflection to achieve an instrument elevation coverage of ±45° for energies up to ~5 keV. Above 5 keV, the elevation coverage is reduced proportional to ion energy due to high-voltage constraints and reaches ±7° at 30 keV. Figure 3b shows the dependence of the elevation coverage of SWIA and STATIC on the measured ion energy.

SWIA and STATIC complete one full energy and elevation sweep every 4 s; however, due to data telemetry rate constraints, ion distributions are typically binned and downsampled in energy, azimuth, elevation, mass, and/or time before downlink. For the pickup ion model-data comparisons provided in this paper,

SWIA's coarse data products are used in which each of the two neighboring energy bins are grouped together (averaged), resulting in 48 energy bins; the 10 fine anodes are binned in groups of 5, resulting in two 22.5° bins in the solar wind direction, which in addition to the 14 coarse anodes create a total of 16 azimuth bins of 22.5°, and there are four elevation bins with a resolution of 22.5°. When MAVEN is in the solar wind, the focus of SWIA is on fine solar wind measurements. Therefore, a smattering of coarse ion distributions, which are acquired in 4 s sweeps and include pickup ion signatures, are telemetered every 8, 16, 32, or 64 s, depending on the telemetry rate availability. The SWIA instrument characteristics, its inflight performance, the science results, and the sources of uncertainty in its measurements are discussed in *Halekas et al*. [2017]. For STATIC, the "D1" data product is used in our model-data comparisons. The D1 data product includes 32 energy bins, 16 azimuth bins, 4 elevation bins, and 8 ion mass bins, with a time resolution of 16 s when MAVEN is in the upstream solar wind and when the instrument is in the "pickup mode" [*McFadden et al*., 2015].

During solar particle events associated with the passage of corotating interaction regions or coronal mass ejections, energetic particle fluxes detected by SEP can become comparable to or even exceed pickup O^+ fluxes [*Jakosky et al*., 2015b; *Lillis et al*., 2016; *Lee et al*., 2017], complicating analysis of pickup O^+ in SEP. Moreover, the field of view (FOV) of each SEP aperture spans about 3% of the whole sky, meaning that each SEP sensor measures only a small part of the pickup ion distribution at a given time, probing a small exospheric hot oxygen altitude range. SWIA and STATIC measure three-dimensional distributions of pickup ions and cover a much larger fraction of the sky compared to SEP. At their full instrument elevation coverage (±45° below 5 keV), about 70% of the sky is covered in all 64 look directions of SWIA and STATIC. This coverage is reduced at higher energies, reaching ~15% of the sky at 25 keV, essentially reducing the angular coverage to within a 2-D plane. This wider coverage compared to SEP allows for constraining exospheric neutral densities over a wider range of altitudes using measured pickup ion fluxes. However, due to their lower energy coverage and geometric factor compared to SEP, only pickup ions that are created within a few R_M can be detected by SWIA and STATIC.

SWIA is mounted on the spacecraft body and oriented such that the bulk of the solar wind ions is almost always within the FOV of its fine angular resolution anodes, thereby allowing SWIA to measure precise solar wind moments when MAVEN is in the upstream solar wind [*Halekas et al*., 2015a]. SWIA's sunward hemisphere look directions also provide an unobstructed view of pickup ions created upstream of Mars and outside the bow shock. STATIC is mounted on MAVEN's Articulated Payload Platform (APP), giving it more flexibility in pointing and allowing it to measure ram ions during MAVEN periapsis passes and pickup ions near the apoapses [*McFadden et al*., 2015]. Also mounted on the APP are the NGIMS (Neutral Gas and Ion Mass Spectrometer) [*Mahaffy et al*., 2015a] and IUVS instruments, which share pointing requirements with STATIC. As a consequence, part of STATIC's FOV can at times be blocked by the spacecraft body, the APP itself, and the instruments mounted on the APP. Also, at certain APP orientations, part of the pickup ion ring beam distribution can lie outside of STATIC's FOV. Nonetheless, SEP, SWIA, and STATIC act as complementary particle detectors, each measuring a distinct part of pickup ion energy/angle distribution.

4. Model-Data Comparisons

Unlike the SEP instrument, which requires solar wind speeds above ~450 km/s to be able to detect pickup O^+ above ~60 keV, SWIA and STATIC detect lower energy pickup ions during almost every orbit. Therefore, when the solar wind speed is high, SWIA and STATIC miss most of the pickup O^+ energy distribution. To put SWIA and STATIC measurements in context with measurements of SEP pickup O^+, we start our model-data comparison by analyzing an orbit during which all three instruments were detecting pickup ions.

4.1. Orbit #350

On 3 December 2014 between 22:00 and 23:00 UTC when MAVEN was near the apoapsis of orbit #350, SEP, STATIC, and SWIA all detected pickup ions at the same time. The average solar wind speed for this time period was 570 km/s, with a proton density of 2.5 cm^{-3}, and an IMF strength of 3.5 nT. The IMF was mainly directed toward the +*Z* direction in MSO coordinates (Mars-Solar-Orbital, in which *X* points from Mars toward the Sun, *Y* is directed opposite to the orbital velocity of Mars, and *Z* completes the right-handed coordinate system).

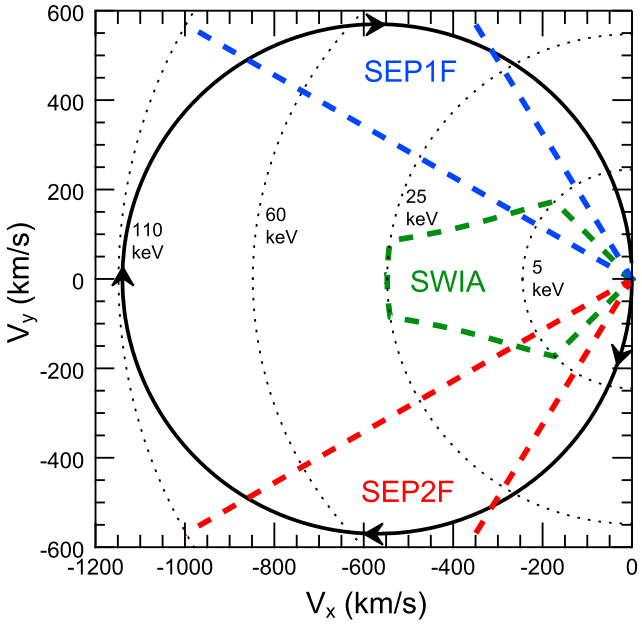

Figure 4. Ring beam distribution of oxygen pickup ions in velocity space for 3 December 2014, 22:00–22:30 UTC. The reversed FOVs of SEP1F, SEP2F, and SWIA are shown by the blue, red, and green dashed lines, respectively. The four dotted curves from right to left represent pickup oxygen constant energy contours of 5, 25, 60, and 110 keV. Note that since SEP's lower energy threshold for detection of oxygen is 60 keV, SEP can only detect pickup O^+ on the ring beam distribution to the left of the 60 keV dotted curve; thus, the blue and red dashed lines only represent an energy-independent angular coverage for SEP, whereas SWIA's elevation coverage is shown to decrease with energy from 5 keV to 25 keV. Since STATIC's orientation is not fixed with respect to SEP and SWIA, STATIC's FOV is not included in this figure.

According to $\boldsymbol{E} = -\boldsymbol{U_{sw}} \times \boldsymbol{B}$, this would create a motional electric field in the $-Y$ direction with a strength of ~2 V/km. The newly created pickup ions accelerate in the direction of the motional electric field and gyrate about the magnetic field, forming a ring beam distribution in velocity space (Figure 4). Thus, for the selected time period, pickup ions start their gyration in the $-Y$ direction, and as they gain energy, their $-X$ velocity component also increases. At the peak of their energy (the half-point in one full gyroperiod), pickup ions will have only a $-X$ velocity component, and after that, their $-X$ velocity component decreases and they gain a $+Y$ velocity component.

Figure 4 depicts this ring beam distribution of pickup ions (black curve) in velocity space, and the arrows on the ring represent the direction in which pickup ion velocities evolve in time. The dotted curves from right to left are constant energy contours of 5, 25, 60, and 110 keV for pickup O^+. The energies are a factor of 16 lower for pickup H^+. The projected FOVs of SEP1F, SEP2F, and SWIA on the V_x-V_y plane are also shown by the blue, red, and green dashed lines, respectively. The letter "F" in SEP1F and SEP2F denotes the forward looking SEP detectors, which typically have look directions in the sunward hemisphere. Note that the look directions shown in the figure have been reversed in sign in order to correspond to the velocity direction of pickup ions that are moving toward each detector. Also, note that SEP can only detect pickup O^+ on the ring beam distribution to the left of the 60 keV dotted curve (>60 keV). The reduction in SWIA's FOV at high energies (from 5 keV to 25 keV) is also shown, and as seen, SWIA's FOV does not overlap with any part of the pickup O^+ ring beam distribution. Therefore, SWIA was not detecting pickup O^+ for the selected time period. The FOV of STATIC is not included in Figure 4, as STATIC is mounted on the spacecraft's APP and its orientation is not fixed with respect to SEP and SWIA. The look directions shown in Figure 4 are valid between 22:00 and 22:30 UTC, after which MAVEN's attitude changed.

Figure 5 shows pickup oxygen data and model results for the same time period. The first four panels in Figure 5 are data and model results for SEP1F and SEP2F, respectively. Between 22:00 and 22:30 UTC as shown in Figure 4, MAVEN's attitude was such that SEP2F had a $[+X, +Y]$ look direction, allowing it to detect oxygen pickup ions that according to the pickup ion model were created ~8 R_M upstream of Mars and were moving toward SEP2F in the $[-X, -Y]$ direction (part of the ring beam distribution in Figure 4 enclosed between the red dashed lines with energies above 60 keV). The exospheric hot oxygen density at 8 R_M, according to *Rahmati et al.* [2014], is ~10 cm^{-3}, and as seen in the color spectrograms of Figure 5, the agreement to within a factor of 2 between the SEP measured and modeled fluxes indicates that for this time period, the actual exospheric density and the associated hot oxygen escape rate were well represented by the exospheric model used in the pickup ion code.

For the same time period, SEP1F had a $[+X, -Y]$ look direction and was detecting oxygen pickup ions that were created ~40 R_M upstream, were past half of their gyroperiod, and had a $[-X, +Y]$ velocity component when detected by SEP1F (part of the ring beam distribution in Figure 4 enclosed between the blue dashed

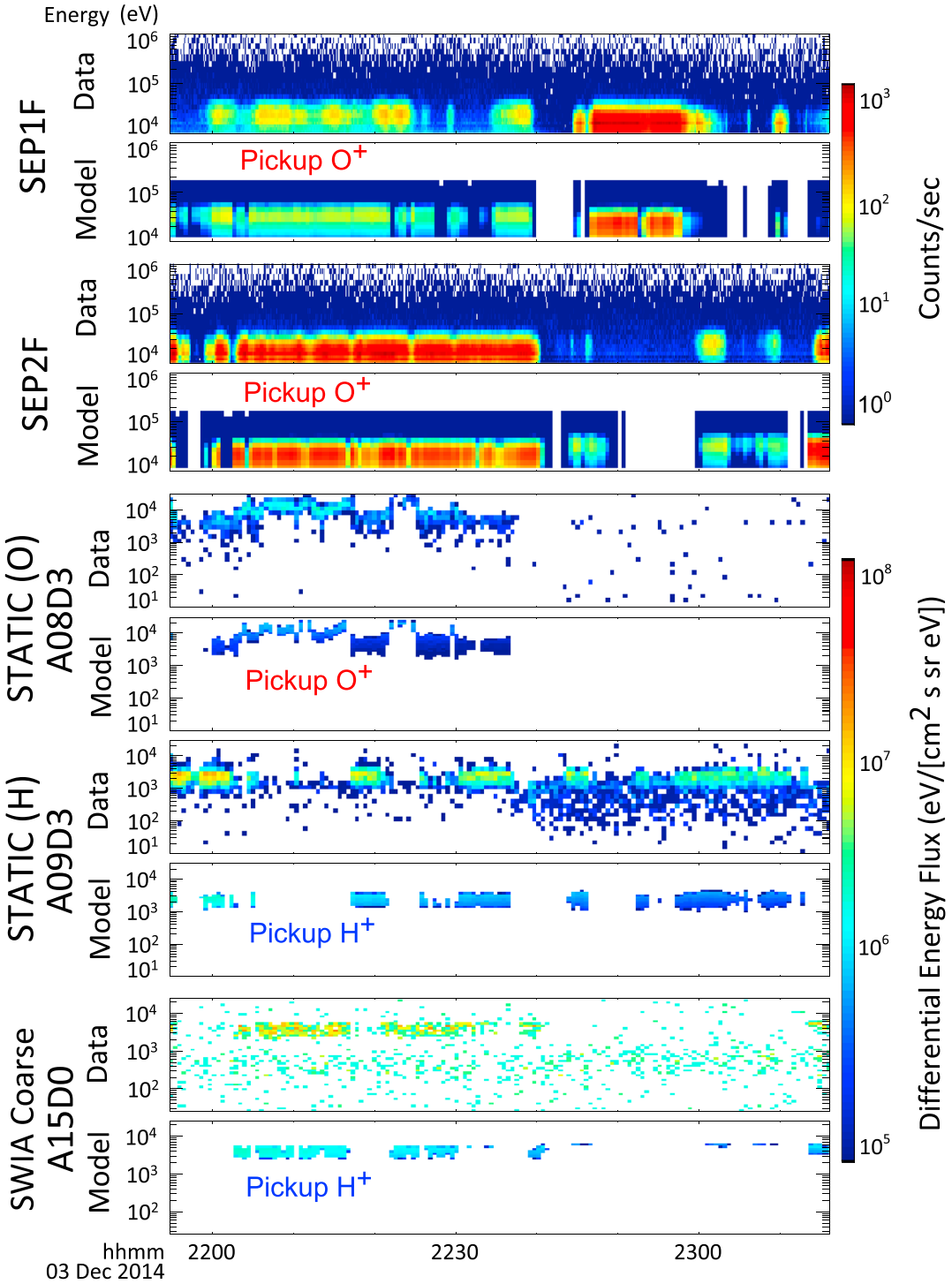

Figure 5. Model-data comparisons of pickup ions measured by SEP1, SEP2, STATIC mass 16 (oxygen), STATIC mass 1 (hydrogen), and SWIA on 3 December 2014, 22:00–23:15 UTC. STATIC and SWIA data/model are for one of the look direction bins of each instrument that contained significant parts of the pickup ion distribution. For pickup O^+ measured by SEP and STATIC, the agreement between the data and modeled fluxes are to within a factor of 2. Pickup H^+ fluxes measured by STATIC and SWIA are, however, underestimated in the model by a factor of ~5. Note that for the shown time period, SWIA did not have any part of the pickup O^+ in its FOV.

lines with energies above 60 keV). Consequently, SEP1F was probing the hot oxygen exospheric densities at a much greater distance from Mars compared to SEP2F, and this is the reason the measured and modeled fluxes are about an order of magnitude lower for SEP1F compared to SEP2F. According to the hot oxygen density profile of *Rahmati et al*. [2014], atomic oxygen number density is 0.5 cm^{-3} at 40 R_M. This is the first time an instrument has been able to probe, although indirectly, such low neutral densities at such great distances from Mars. For the discussed time period, oxygen pickup ions that were within the FOV of the two SEPs had energies between 30 and 80 keV, but only those above ~60 keV deposit up to 40 keV in the silicon detectors, as seen in the energy response shown in Figure 3a. Although oxygen pickup ions had a maximum energy of 110 keV, those close to their maximum energy were outside the FOV of both SEPs. For other time periods, as discussed in *Rahmati et al*. [2015], given favorable solar wind and FOV conditions, SEP would be able to probe oxygen pickup ions at or near their maximum energy.

SWIA and STATIC, with maximum detection energies of 25 and 30 keV, respectively, often miss the high-energy part of the pickup O^+ energy distribution. The fifth and sixth panels in Figure 5 show measured and modeled pickup O^+ energy fluxes for one of the look direction bins of STATIC (22.5° × 22.5°) that had part of the pickup O^+ distribution in its FOV. According to the naming convention used in the pickup ion code, the selected look direction bin is for azimuth bin #09 and elevation (or deflection) bin #3, denoted in the figure as A08D3. The detected oxygen pickup ions in this look direction of STATIC were born between 1 and 4 R_M upstream of MAVEN and were in the beginning of their cycloid motion, accelerating in the direction of the motional electric field. STATIC therefore probes the Martian hot oxygen exosphere at distances much closer to Mars compared to SEP. The agreement, to within a factor of 2, between the model results and the data indicates that the assumed exospheric hot oxygen density profile in the pickup ion model is representative of the actual conditions for the selected time period.

The seventh and eighth panels in Figure 5 show data and model results for another look direction bin of STATIC, namely, A09D3, which had part of the pickup H^+ distribution in its FOV. Since pickup hydrogen gyroradii are comparable to the Martian radius, and therefore, to the scale height of the hydrogen exosphere, the pickup ion model is set to integrate the pickup H^+ fluxes over several gyroperiods to ensure that the full source of pickup H^+ is captured in the model. Nevertheless, comparing the flux levels shows that the model underestimates the fluxes by a factor of ~5. This discrepancy in flux levels suggests that the assumed exospheric hydrogen density profile adapted from *Feldman et al*. [2011] underestimates the actual neutral hydrogen densities for the selected time period by a factor of ~5.

The ninth and tenth panels in Figure 5 show the measured and modeled energy fluxes of pickup H^+ detected in one of the coarse look direction bins of SWIA (22.5° × 22.5°), namely, A15D0. As seen, the modeled pickup H^+ fluxes are again lower than the measured ones by about a factor of 5. Although the upstream conditions were relatively stable for the selected time period, due to the small FOV of each bin of SWIA and STATIC (~1% of the sky), even the slightest change in the direction of the IMF takes pickup ions in and out of the FOV of each bin, and this effect is well captured in the model. As discussed earlier and shown in Figure 4, for the selected time period no part of the pickup O^+ distribution was within the energy range and FOV of SWIA. The background counts seen in the SWIA data are mainly the scattered solar wind ions in the instrument. Also, for the selected time period, SWIA's attenuator was closed, reducing its geometric factor by about an order of magnitude [*Halekas et al*., 2015a], and this is the reason the lower limit level of noise in the shown SWIA data is relatively high.

4.2. Orbit #438

We now turn our focus to SWIA for studying another MAVEN orbit, during which SWIA detected both pickup O^+ and H^+. Similar to STATIC, oxygen pickup ions detected by SWIA are created at distances within a few R_M, and model-data comparisons help in constraining the mainly bound component of the hot oxygen exosphere. Figure 6 shows MAVEN data for a 2 h time period of orbit #438 on 20 December 2014 from 17:30 to 19:30 UTC. For this time period, MAVEN was in the solar wind, SWIA's attenuator was open, and SWIA measured a solar wind velocity of ~360 km/s, too low for SEP detection of pickup O^+. The IMF components measured by the MAG instrument are shown in the first panel in MSO coordinates. The IMF magnitude is ~5 nT, but as seen, its individual components are quite variable, creating a dynamic pickup ion distribution. The second panel shows the maximum energy that oxygen pickup ions can acquire, calculated according to

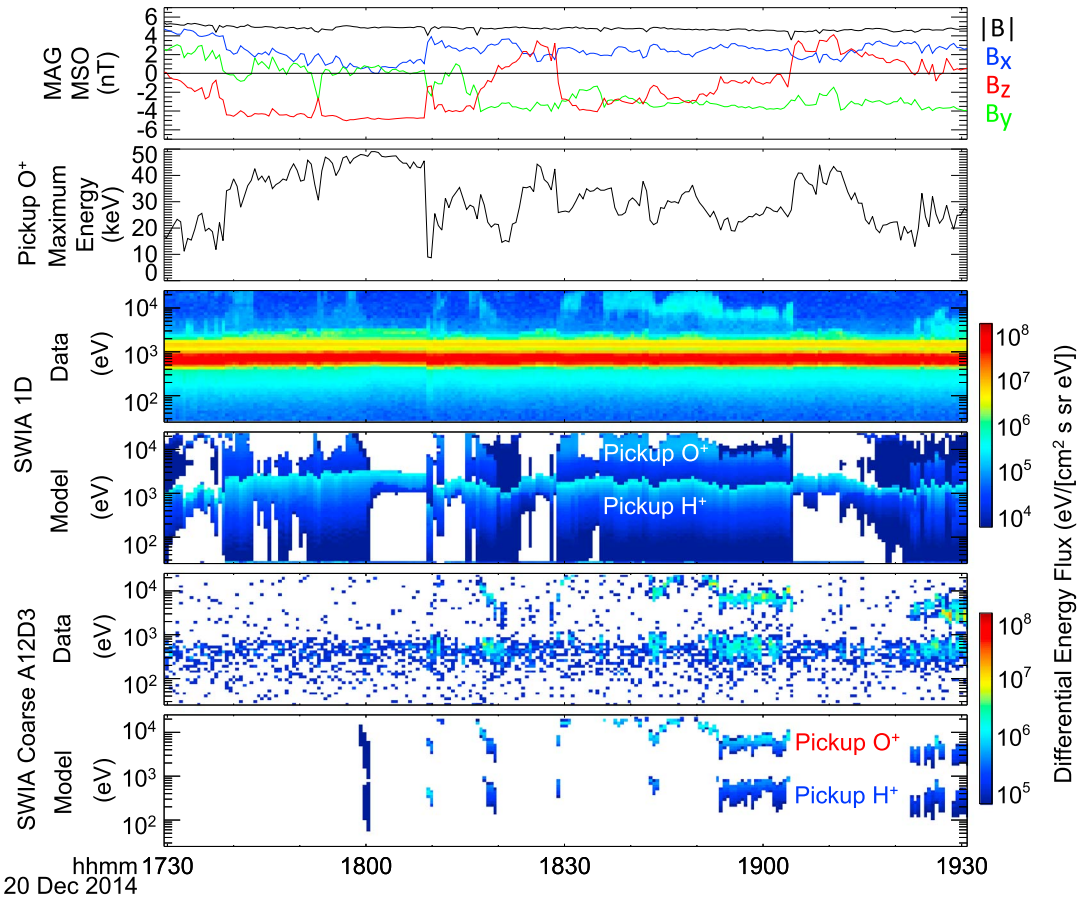

Figure 6. Mode-data comparisons of hydrogen and oxygen pickup ions measured by SWIA on 20 December 2014, 17:30–19:30 UTC. (top to bottom) Magnetometer measurements of the magnetic field in MSO coordinates, calculated maximum energy of oxygen pickup ions, angle-averaged (1-D) SWIA data, angle-averaged (1-D) SWIA pickup ion model, directional SWIA data, and directional SWIA pickup ion model. The last two panels show one of the look direction bins of SWIA that includes both pickup H^+ and O^+ but does not include the solar wind in its FOV. The agreement between pickup O^+ fluxes in the data and in the model results is to within a factor of 2. Modeled pickup H^+ fluxes are too low by a factor of ~5 compared to the data.

$E_{max} = 2\,m\,U_{sw}{}^2\,\sin^2(\theta_{UB})$, where m is the mass of the pickup ion (in this case oxygen), U_{sw} is the solar wind speed, and θ_{UB} is the IMF cone angle, or the angle between the magnetic field and the solar wind velocity. As seen, pickup O^+ energies are below 50 keV, making them too low energy to be detected by SEP.

SWIA's angle-averaged (one-dimensional or 1-D) energy-time spectrogram and the associated pickup ion model results are shown in the third and fourth panels in Figure 6, respectively. The 1-D spectra are calculated on board the instrument by summing the counts over all the look directions of SWIA. Solar wind protons and alpha particles are seen at energies of ~700 eV and ~1400 eV, respectively, in the data panel. The model panel only includes simulated pickup ions and does not show the solar wind ions. Pickup O^+ fluxes are seen in both the data, and the model results at energies above a few keV; however, pickup H^+ spectra are mostly buried under the solar wind ion fluxes in the 1-D data. The fifth and sixth panels in Figure 6 show data and model results for only one of the look directions of SWIA, namely, A12D3, which did not have the solar wind ions in its FOV but had both pickup O^+ and pickup H^+ populations in its FOV. This directional analysis of SWIA data allows for precise determination of the angular distribution of pickup ions. For the chosen look direction, pickup H^+ spectra are no longer being masked by the intense solar wind ion fluxes.

As seen in Figure 6, the pickup ion model used in this study again predicts the time variation of oxygen and hydrogen pickup ion spectra fairly accurately. Since SWIA's attenuator was open during the selected time period, the lower limit level of background counts is about an order of magnitude lower than the lower limit noise level present in the ninth panel of Figure 5. Also, similar to the time period shown in

Figure 5, pickup H^+ fluxes in the model are again a factor of ~5 lower than the data, indicating that the assumed exospheric hydrogen of *Feldman et al*. [2011] exhibits too low of a density for the selected time period. The case studies presented so far correspond to near-solar maximum conditions and when Mars was near its perihelion, as orbits #350 and #438 correspond to solar longitudes $L_S = 245°$ and 255°, respectively, with a heliocentric distance of 1.38 AU. The *Feldman et al*. [2011] density profile, however, corresponds to observations made on 25 February 2007 when Mars was at solar longitude $L_S = 190°$, with a heliocentric distance of 1.44 AU, and near-solar minimum. Note that SWIA's attenuator was closed during most of the orbits near the perihelion, due to high solar wind fluxes. However, during most of orbit #438, SWIA's attenuator was open and SWIA detected pickup O^+. In order to assess the role of heliocentric distance and/or Mars season on exospheric densities, we carry out another model-data comparison for an orbit during aphelion conditions.

4.3. Orbit #2427

For the time period near the Mars aphelion ($L_S \sim 70°$), which occurred in mid-November 2015, MAVEN's orbit geometry was such that no upstream solar wind measurement was available, rendering pickup ion modeling impossible. We therefore study a time period just after the aphelion when MAVEN was back in the upstream solar wind. Figure 7 shows SWIA model-data comparisons for a 1.5 h time period of orbit #2427 on 29 December 2015. For this date, Mars was at $L_S = 88°$, which is 40 days past aphelion, with a heliocentric distance of 1.66 AU. The first three panels of Figure 7 are similar to those of Figure 6. As seen in the first panel, the IMF is more steady compared to orbit #438, with a magnitude of ~2.5 nT. The measured solar wind velocity was ~300 km/s, giving pickup O^+ maximum energies that are below 30 keV (shown in the second panel), again too low for SEP to detect pickup O^+. As seen in the third panel of Figure 7, pickup ion signatures are hard to distinguish in SWIA's 1-D spectra, due to their low fluxes compared to the solar wind and background counts. The last four panels in Figure 7 show a pair of model-data comparisons for two of the neighboring look direction bins of SWIA's coarse data product, namely, A12D2 and A13D2. The A12D2 look direction is probing pickup ions that are newly born and are less energized compared to the ones detected in the A13D2 look direction. The flux levels agree to within a factor of 2 between the data and the model results, for both pickup O^+ and pickup H^+, indicating that exospheric hydrogen densities must have dropped compared to orbit #438, bringing them more in line with the *Feldman et al*. [2011] density profile. In the next section we show how these SWIA model-data comparisons can be used to constrain altitude profiles of hot oxygen and thermal hydrogen neutral atoms outside the Martian bow shock.

5. Constraining Exospheric Neutral Densities

As discussed before, energetic pickup O^+ measurements of SEP can be used to place constraints on the mainly escaping oxygen atoms. SWIA and STATIC measure lower energy pickup O^+ and H^+ and are able to constrain lower altitude exospheric densities. Figure 8 shows reconstructed altitude profiles of neutral oxygen and hydrogen densities in the Mars exosphere, obtained from SWIA pickup ion measurements during orbits #438 and #2427 (the same time periods shown in Figures 6 and 7, respectively). The altitude profiles are constructed by a reverse method that uses measured to modeled pickup ion flux ratios in each time/energy/azimuth/elevation bin of SWIA, which would give a direct link to the source density at the birth location of the measured pickup ions. The source location is calculated in the pickup ion code, and a density is assigned to each point based on the measured to modeled pickup ion flux ratio, since pickup ion fluxes are directly proportional to their neutral source densities. The retrieved density points are then binned in altitude. At each altitude bin, the standard deviation of the retrieved densities, their mean, and the standard error of the mean are calculated. These values are shown in Figure 8, and also included for comparison are the two original altitude profiles used as the neutral source in the pickup ion code (dotted lines).

Note that in our error analysis, the uncertainties in upstream parameters are not propagated to the densities, nor are instrument systematic errors included. The statistics are purely calculated from the variation of the retrieved density points. The standard deviations (dashed lines) in the retrieved density points span almost an order of magnitude in density for both oxygen and hydrogen. It is highly unlikely that such large fluctuations are present in the actual exospheric densities at such high altitudes. The root cause of the rather large standard deviation in the derived densities is the uncertainties present in the measurements of the upstream drivers.

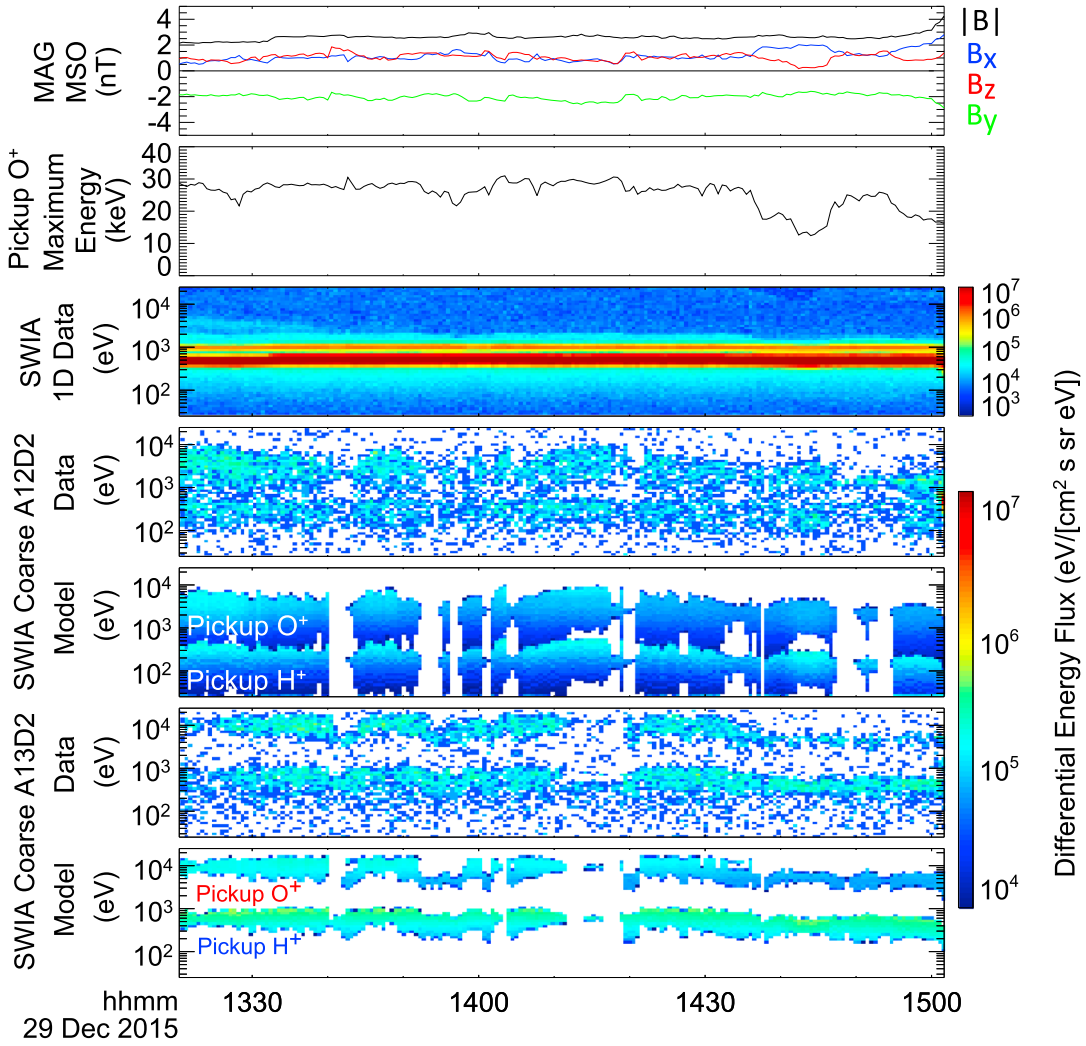

Figure 7. Mode-data comparisons of hydrogen and oxygen pickup ions measured by SWIA on 29 December 2015, 13:20–15:00 UTC. The first three panels are described in Figure 6. The last four panels are a pair of model-data comparisons for two of the neighboring look direction bins of SWIA that include both pickup H^+ and O^+ but do not include the solar wind in their FOV. The agreement between both pickup H^+ and O^+ in the data and the model results is to within a factor of 2.

Since each look direction (22.5° × 22.5°) and energy bin ($\Delta E/E \sim 14\%$) of SWIA only probes a very small part of the pickup ion distribution, the slightest error in the measured upstream field vectors can result in the simulated pickup ions being placed in the wrong instrument bin in the model. Nevertheless, averaging over several retrieved densities results in mean densities with standard errors (solid lines) spanning over less than a factor of 2 in density.

For perihelion conditions, Figure 8a shows that the mean hot oxygen densities for orbit #438 match the assumed density profile of *Rahmati et al.* [2014] to within a factor of 2, indicating that hot oxygen exosphere calculations of *Rahmati et al.* [2014], with their reported escape flux of $9 \times 10^7\ cm^{-2}\ s^{-1}$ and escape rate of $7 \times 10^{25}\ s^{-1}$, are valid representations of actual conditions for this time period. Reconstructed hydrogen densities, however, are about a factor of 5 higher than the *Feldman et al.* [2011] density profile, the same difference factor that is seen in the pickup H^+ flux model-data comparisons presented in Figure 6. As mentioned above, since pickup H^+ gyroradii at Mars are comparable to the scale height of the hydrogen exosphere, the pickup ion code needs to solve multiple pickup hydrogen gyroperiods to ensure that the neutral source of pickup ions is fully captured in the model. In the reverse method, however, the code only solves one gyroperiod in order to be able to assign a single source point to the measured pickup ions in each SWIA bin. This would underestimate the modeled pickup H^+ fluxes by up to 30% for this time period, overestimating the

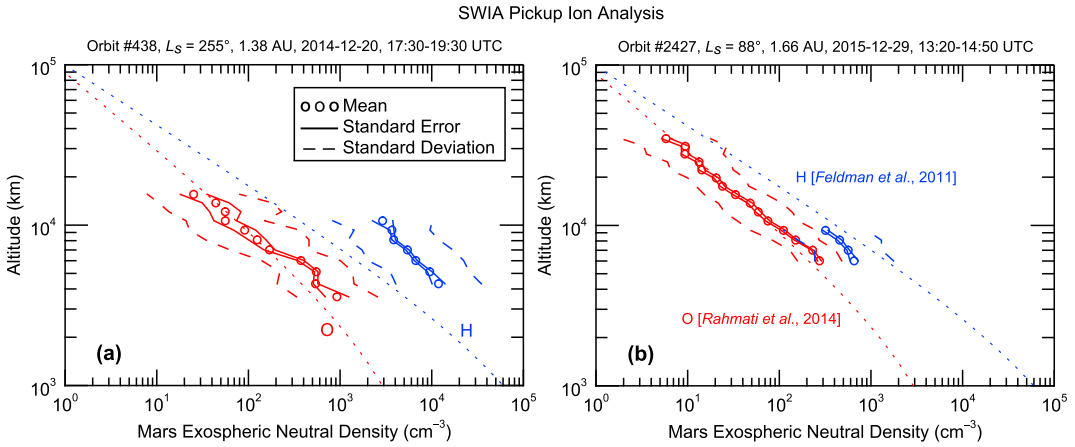

Figure 8. Reconstructed oxygen and hydrogen exospheric density profiles using model-data comparisons of SWIA measured pickup O^+ and H^+ for (a) orbit #438 on 20 December 2014, 17:30–19:30 UTC, close to perihelion and (b) orbit #2427 on 29 December 2015, 13:20–14:50 UTC, near aphelion. Oxygen densities agree to within a factor of 2 with the input exospheric density of *Rahmati et al.* [2014], suggesting a robust oxygen exosphere. An order of magnitude drop in hydrogen densities over half a Martian year is observed. For comparison, model input exospheric profiles shown in Figure 2a are also included as dotted lines.

reconstructed densities by the same factor. This overestimation is, however, well below the factor of 5 difference in the hydrogen densities. It is seen in Figure 8b that hydrogen densities have decreased by an order of magnitude from perihelion to aphelion, whereas the oxygen exosphere has remained more or less the same. This shows that the hydrogen exosphere at Mars is more strongly influenced by heliocentric distance and/or season compared to the hot oxygen exosphere.

Figure 8 shows good agreement between the *Rahmati et al.* [2014] modeled hot O densities and the densities inferred from the MAVEN pickup ion SWIA data, including at large radial distances (greater than 10^4 km). Similarly, *Rahmati et al.* [2015] and *Rahmati* [2016] showed good agreement between modeled pickup O^+ fluxes and fluxes measured by the SEP instrument. As discussed earlier, oxygen pickup ions measured by SEP are dominated by ions that originate at radial distances where the escape component of the hot O velocity distribution starts to become important. Given that modeled and measured hot O densities agree rather well, it is unlikely that the hot O escape rate determined by *Rahmati et al.* [2014] could be too far off and thus provides a preliminary constraint on hot O escape rates. However, a more systematic study of oxygen and hydrogen escape rates using both the pickup ion technique and the MAVEN IUVS measurements of the oxygen and hydrogen corona [e.g., *Lee et al.*, 2015b; *Chaffin et al.*, 2015; *Clarke et al.*, 2017] should be undertaken.

6. Discussion

Models of the Martian hydrogen exosphere suggest that strong solar cycle and seasonal variations exist in exospheric hydrogen densities, driven by the change in the solar EUV flux reaching Mars [e.g., *Chaufray et al.*, 2015]. Recent observations also imply that the hydrogen exosphere at Mars exhibits a significant variation on time scales ranging from weeks to years. This variation has been observed in the Lyman α measurements of the Mars hydrogen exosphere by the Hubble Space Telescope [*Clarke et al.*, 2014; *Bhattacharyya et al.*, 2015] and also by the ultraviolet spectrometers on Mars Express [*Chaffin et al.*, 2014] and MAVEN [*Clarke et al.*, 2017], as well as the ASPERA-3 measurements of hydrogen pickup ions [*Yamauchi et al.*, 2015b]. More recently, SWIA observations of precipitating solar wind protons in the Mars thermosphere [*Halekas et al.*, 2015b] also pointed to an order of magnitude seasonal change in the column density of the hydrogen exosphere outside the bow shock [*Halekas et al.*, 2017]. The occurrence rate of proton cyclotron waves excited by hydrogen pickup ions and observed by MAVEN upstream of Mars also decreased from perihelion to aphelion [*Romanelli et al.*, 2016], indicating a drop in the hydrogen exosphere. Our pickup H^+ model-data comparisons also reveal an order of magnitude change in the density of the Martian hydrogen exosphere as measured by SWIA and STATIC.

When Mars is near its aphelion, the pickup H^+ flux can fall below the detection threshold of SWIA and STATIC, particularly when the instrument attenuators are closed. Part of this drop in pickup H^+ flux levels can be associated with the reduction in the ionization frequency of the neutral hydrogen exosphere, due to the lower solar EUV and solar wind flux reaching Mars near aphelion, thus lowering the production rate of pickup H^+. The solar EUV and solar wind fluxes are both inversely proportional to the square of the Sun-Mars distance, and as this distance increases by a factor of 1.2 from perihelion to aphelion, the reduction in ionization frequencies can be as large as a factor of 1.45. The reduction in the IMF magnitude also plays a role in lowering pickup ion fluxes. The IMF magnitude is statistically inversely proportional to the Sun-Mars distance, and pickup ion gyroradii are inversely proportional to the IMF magnitude. Therefore, lowering the IMF magnitude by a factor of 1.2 from perihelion to aphelion would increase pickup H^+ gyroradii by the same factor, which means that pickup ions reaching MAVEN with the same energy would be created at larger distances from Mars where neutral densities are lower. According to the *Feldman et al*. [2011] hydrogen density profile, a factor of 1.2 increase in the distance between MAVEN and the source of pickup H^+ would lower pickup H^+ fluxes by a factor of 1.3. Thus, the combined effects of the reduction in both the ionization frequencies and the IMF magnitude can alone decrease pickup H^+ fluxes by a factor of 1.9. These effects are all included in the pickup ion code used in this study, as the code uses measured upstream values for the IMF and solar wind to calculate pickup ion ionization frequencies and trajectories. The order of magnitude change in the hydrogen exosphere as indicated by our pickup H^+ analysis can therefore be only attributed to an actual order of magnitude change in hydrogen densities in the exosphere of Mars.

The 30.4 nm EUV irradiance at Mars, which is a good proxy for variations in the photoionization frequency, was 3.2×10^{-4} W/cm^2/nm for orbit #438 and 1.9×10^{-4} W/cm^2/nm for orbit #2427, as modeled by the FISM, based on the data from the EUVM instrument [*Thiemann et al*., 2017]. The drop in the EUV irradiance from December 2014 to December 2015 was not only due to the increase in the heliocentric distance from perihelion to aphelion but was also influenced by the declining phase of solar cycle #24 [*Thiemann et al*., 2017]. As the analytical approach of *Cravens et al*. [2017] demonstrates, the hot oxygen escape flux and thus exospheric oxygen densities at Mars should be directly proportional the incident solar EUV irradiance, thereby varying less than a factor of 2 with Mars season. This rather small variation in the hot oxygen escape is also supported by our pickup O^+ analyses of the SEP, SWIA, and STATIC measurements. The order of magnitude variation of the hydrogen exosphere, however, has only recently come to light, and better understanding of its sources and drivers awaits further investigation.

7. Conclusions

The pickup ion model used in this study proves successful in simulating the time variation of oxygen and hydrogen pickup ion distributions outside the Martian bow shock under a wide range of upstream solar wind conditions. We analyzed pickup ion data from the SEP, SWIA, and STATIC instruments on the MAVEN spacecraft and used a pickup ion model to conduct model-data comparisons of pickup O^+ and H^+ fluxes at Mars. Our analysis of the pickup O^+ data confirms that a hot oxygen exosphere exists on Mars, extending to tens of R_M. We showed that the two forward looking SEP detectors are able to measure oxygen pickup ions that are created tens of R_M upstream, thus probing the hot oxygen density at altitudes not accessible before. Since the density of escaping hot oxygen atoms dominates over the gravitationally bound oxygen exosphere at altitudes greater than ~10 R_M, an analysis of SEP pickup O^+ data, as discussed, can constrain model simulations of the Mars far exosphere and neutral oxygen escape rates. Comparisons of pickup O^+ fluxes measured by SEP with the hot oxygen exospheric model of *Rahmati et al*. [2014] constrain to within a factor of 2 the hot oxygen escape rate at Mars to be 7×10^{25} s^{-1}. The SWIA and STATIC instruments detect pickup O^+ and H^+ ions that are created closer to Mars and are in the beginning of their cycloid motion. Pickup O^+ fluxes measured by SWIA and STATIC are consistent with pickup O^+ model simulations, indicating that the assumed exospheric oxygen density profile of *Rahmati et al*. [2014] used in the pickup ion model is good to within a factor of 2 for the time periods studied. An analysis of pickup H^+ measured by SWIA and STATIC, however, reveals an order of magnitude change in the hydrogen exosphere with Mars season, reaffirming previous modeling and observations of the presence of a nonlinear relation between the incident solar EUV flux and hydrogen escape at Mars. In order to constrain hydrogen escape rates, hydrogen exosphere models such as the one discussed in *Chaffin et al*. [2015] need to be compared with our pickup ion constructed densities. In

future work, we will apply the same methodology to a larger number of MAVEN orbits with favorable upstream conditions, in order to carry out a statistical analysis of exospheric densities and escape rates, which will allow us to draw conclusions on the dynamic range of the variability of atmospheric escape at Mars with time.

Acknowledgments
The MAVEN project is supported by NASA through the Mars Exploration Program. G.A.D. was supported by a NASA Postdoctoral Program appointment at the NASA Goddard Space Flight Center, administered by Universities Space Research Association through a contract with NASA. With special thanks to J.E. Connerney for his contributions toward the availability of high-quality MAG data. MAVEN data are publicly available through the Planetary Data System. The source code for the pickup ion model used this study is publicly available at http://goo.gl/Fctdzi. The authors wish to thank two anonymous reviewers for their constructive comments, which helped enhance the quality of this paper.

References

Acton, C. H. (1996), Ancillary data services of NASA's Navigation and Ancillary Information Facility, *Planet. Space Sci.*, *44*(1), 65–70, doi:10.1016/0032-0633(95)00107-7.

Anderson, D. E. (1974), Mariner 6, 7, and 9 Ultraviolet Spectrometer Experiment: Analysis of hydrogen Lyman alpha data, *J. Geophys. Res.*, *79*(10), 1513–1518, doi:10.1029/JA079i010p01513.

Anderson, D. E., and C. W. Hord (1971), Mariner 6 and 7 Ultraviolet Spectrometer Experiment: Analysis of hydrogen Lyman-alpha data, *J. Geophys. Res.*, *76*(28), 6666–6673, doi:10.1029/JA076i028p06666.

Andrews, D. J., L. Andersson, G. T. Delory, R. E. Ergun, A. I. Eriksson, C. M. Fowler, T. McEnulty, M. W. Morooka, T. Weber, and B. M. Jakosky (2015), Ionospheric plasma density variations observed at Mars by MAVEN/LPW, *Geophys. Res. Lett.*, *42*, 8862–8869, doi:10.1002/2015GL065241.

Angel, G. C., and J. A. Samson (1988), Total photoionization cross sections of atomic oxygen from threshold to 44.3 Å, *Phys. Rev. A*, *38*(11), 5578, doi:10.1103/PhysRevA.38.5578.

Barabash, S., E. Dubinin, N. Pissarenko, R. Lundin, and C. T. Russell (1991), Picked-up protons near Mars: Phobos observations, *Geophys. Res. Lett.*, *18*(10), 1805–1808, doi:10.1029/91GL02082.

Barth, C. A., C. W. Hord, J. B. Pearce, K. K. Kelly, G. P. Anderson, and A. I. Stewart (1971), Mariner 6 and 7 Ultraviolet Spectrometer Experiment: Upper atmosphere data, *J. Geophys. Res.*, *76*(10), 2213–2227, doi:10.1029/JA076i010p02213.

Barth, C. A., A. I. Stewart, C. W. Hord, and A. I. Lane (1972), Mariner 9 ultraviolet spectrometer experiment: Mars airglow spectroscopy and variations in Lyman alpha, *Icarus*, *17*(2), 457–468, doi:10.1016/0019-1035(72)90011-5.

Benna, M., P. R. Mahaffy, J. M. Grebowsky, J. L. Fox, R. V. Yelle, and B. M. Jakosky (2015), First measurements of composition and dynamics of the Martian ionosphere by MAVEN's Neutral Gas and Ion Mass Spectrometer, *Geophys. Res. Lett.*, *42*, 8958–8965, doi:10.1002/2015GL066146.

Bhattacharyya, D., J. T. Clarke, J.-L. Bertaux, J.-Y. Chaufray, and M. Mayyasi (2015), A strong seasonal dependence in the Martian hydrogen exosphere, *Geophys. Res. Lett.*, *42*, 8678–8685, doi:10.1002/2015GL065804.

Bougher, S. W., T. E. Cravens, J. Grebowsky, and J. Luhmann (2014), The aeronomy of Mars: Characterization by MAVEN of the upper atmosphere reservoir that regulates volatile escape, *Space Sci. Rev.*, doi:10.1007/s11214-014-0053-7.

Bougher, S. W., et al. (2015), Early MAVEN Deep Dip campaign reveals thermosphere and ionosphere variability, *Science*, *350*(6261), doi:10.1126/science.aad0459.

Bougher, S. W., et al. (2017), The structure and variability of Mars dayside thermosphere from MAVEN NGIMS and IUVS measurements: Seasonal and solar activity trends in scale heights and temperatures, *J. Geophys. Res. Space Physics*, *122*, 1296–1313, doi:10.1002/2016JA023454.

Brain, D. A., et al. (2010), A comparison of global models for the solar wind interaction with Mars, *Icarus*, *206*, 139–151, doi:10.1016/j.icarus.2009.06.030.

Brain, D. A., et al. (2015), The spatial distribution of planetary ion fluxes near Mars observed by MAVEN, *Geophys. Res. Lett.*, *42*, 9142–9148, doi:10.1002/2015GL065293.

Brecht, S. H., and S. A. Ledvina (2006), The solar wind interaction with the Martian ionosphere/atmosphere, *Space Sci. Rev.*, *126*, 15–38, doi:10.1007/s11214-006-9084-z.

Brecht, S. H., and S. A. Ledvina (2010), The loss of water from Mars: Numerical results and challenges, *Icarus*, *206*, 164–173, doi:10.1016/j.icarus.2009.04.028.

Chaffin, M. S., J.-Y. Chaufray, I. Stewart, F. Montmessin, N. M. Schneider, and J.-L. Bertaux (2014), Unexpected variability of Martian hydrogen escape, *Geophys. Res. Lett.*, *41*, 314–320, doi:10.1002/2013GL058578.

Chaffin, M. S., et al. (2015), Three-dimensional structure in the Mars H corona revealed by IUVS on MAVEN, *Geophys. Res. Lett.*, *42*, 9001–9008, doi:10.1002/2015GL065287.

Chamberlain, J. W., and D. M. Hunten (1987), *Theory of Planetary Atmospheres: An Introduction to Their Physics and Chemistry*, Academic Press, Florida.

Chamberlin, P. C., T. N. Woods, and F. G. Chamberlin (2007), Flare Irradiance Spectral Model (FISM): Daily component algorithms and results, *Space Weather*, *5*, S07005, doi:10.1029/2007SW000316.

Chassefière, E., and F. Leblanc (2004), Mars atmospheric escape and evolution: Interaction with the solar wind, *Planet. Space Sci.*, *52*(11), 1039–1058, doi:10.1016/j.pss.2004.07.002.

Chaufray, J. Y., J. L. Bertaux, F. Leblanc, and E. Quémerais (2008), Observation of the hydrogen corona with SPICAM on Mars Express, *Icarus*, *195*(2), 598–613, doi:10.1016/j.icarus.2008.01.009.

Chaufray, J. Y., F. Gonzalez-Galindo, F. Forget, M. Lopez-Valverde, F. Leblanc, R. Modolo, and S. Hess (2015), Variability of the hydrogen in the Martian upper atmosphere as simulated by a 3D atmosphere–exosphere coupling, *Icarus*, *245*, 282–294, doi:10.1016/j.icarus.2014.08.038.

Clarke, J. T., J.-L. Bertaux, J.-Y. Chaufray, G. R. Gladstone, E. Quemerais, J. K. Wilson, and D. Bhattacharyya (2014), A rapid decrease of the hydrogen corona of Mars, *Geophys. Res. Lett.*, *41*, 8013–8020, doi:10.1002/2014GL061803.

Clarke, J. T., et al. (2017), Variability of D and H in the Martian upper atmosphere observed with the MAVEN IUVS Echelle Channel, *J. Geophys. Res. Space Physics*, *122*, doi:10.1002/2016JA023479, in press.

Connerney, J. E. P., J. Espley, P. Lawton, S. Murphy, J. Odom, R. Oliversen, and D. Sheppard (2015a), The MAVEN magnetic field investigation, *Space Sci. Rev.*, doi:10.1007/s11214-015-0169-4.

Connerney, J. E. P., J. R. Espley, G. A. DiBraccio, J. R. Gruesbeck, R. J. Oliversen, D. L. Mitchell, J. Halekas, C. Mazelle, D. Brain, and B. M. Jakosky (2015b), First results of the MAVEN magnetic field investigation, *Geophys. Res. Lett.*, *42*, 8819–8827, doi:10.1002/2015GL065366.

Cravens, T. E. (2004), *Physics of Solar System Plasmas*, Cambridge Univ. Press, Cambridge, U. K.

Cravens, T. E., J. U. Kozyra, A. F. Nagy, T. I. Gombosi, and M. Kurtz (1987), Electron impact ionization in the vicinity of comets, *J. Geophys. Res.*, *92*(A7), 7341–7353, doi:10.1029/JA092iA07p07341.

Cravens, T. E., A. Hoppe, S. A. Ledvina, and S. McKenna-Lawlor (2002), Pickup ions near Mars associated with escaping oxygen atoms, *J. Geophys. Res.*, *107*(A8), 1170, doi:10.1029/2001JA000125.

Cravens, T. E., et al. (2017), Hot oxygen escape from Mars: Simple scaling with solar EUV irradiance, *J. Geophys. Res. Space Physics*, *122*, 1102–1116, doi:10.1002/2016JA023461.

Curry, S. M., M. Liemohn, X. Fang, Y. Ma, and J. Espley (2013), The influence of production mechanisms on pick-up ion loss at Mars, *J. Geophys. Res. Space Physics*, *118*, 554–569, doi:10.1029/2012JA017665.
Curry, S. M., et al. (2014), Test particle comparison of heavy atomic and molecular ion distributions at Mars, *J. Geophys. Res. Space Physics*, *119*, 2328–2344, doi:10.1002/2013JA019221.
Curry, S. M., et al. (2015), Response of Mars O^+ pickup ions to the 8 March 2015 ICME: Inferences from MAVEN data-based models, *Geophys. Res. Lett.*, *42*, 9095–9102, doi:10.1002/2015GL065304.
Deighan, J., et al. (2015), MAVEN IUVS observation of the hot oxygen corona at Mars, *Geophys. Res. Lett.*, *42*, 9009–9014, doi:10.1002/2015GL065487.
Dong, C., S. W. Bougher, Y. Ma, G. Toth, Y. Lee, A. F. Nagy, V. Tenishev, D. J. Pawlowski, M. R. Combi, and D. Najib (2015a), Solar wind interaction with the Martian upper atmosphere: Crustal field orientation, solar cycle and seasonal variations, *J. Geophys. Res. Space Physics*, *120*, 7857–7872, doi:10.1002/2015JA020990.
Dong, Y., X. Fang, D. A. Brain, J. P. McFadden, J. S. Halekas, J. E. Connerney, S. M. Curry, Y. Harada, J. G. Luhmann, and B. M. Jakosky (2015b), Strong plume fluxes at Mars observed by MAVEN: An important planetary ion escape channel, *Geophys. Res. Lett.*, *42*, 8942–8950, doi:10.1002/2015GL065346.
Dostovalov, S. B., and S. D. Chuvakhin (1973), On the distribution of neutral hydrogen in the upper atmosphere of Mars, *Cosmic Res.*, *11*, 767–773.
Dubinin, E., M. Fraenz, J. Woch, S. Barabash, R. Lundin, and M. Yamauchi (2006), Hydrogen exosphere at Mars: Pickup protons and their acceleration at the bow shock, *Geophys. Res. Lett.*, *33*, L22103, doi:10.1029/2006GL027799.
Eparvier, F. G., P. C. Chamberlin, T. N. Woods, and E. M. B. Thiemann (2015), The solar extreme ultraviolet monitor for MAVEN, *Space Sci. Rev.*, doi:10.1007/s11214-015-0195-2.
Ergun, R. E., M. W. Morooka, L. A. Andersson, C. M. Fowler, G. T. Delory, D. J. Andrews, A. I. Eriksson, T. McEnulty, and B. M. Jakosky (2015), Dayside electron temperature and density profiles at Mars: First results from the MAVEN Langmuir probe and waves instrument, *Geophys. Res. Lett.*, *42*, 8846–8853, doi:10.1002/2015GL065280.
Fang, X., M. W. Liemohn, A. F. Nagy, Y. Ma, D. L. De Zeeuw, J. U. Kozyra, and T. H. Zurbuchen (2008), Pickup oxygen ion velocity space and spatial distribution around Mars, *J. Geophys. Res.*, *113*, A02210, doi:10.1029/2007JA012736.
Fang, X., S. W. Bougher, R. E. Johnson, J. G. Luhmann, Y. Ma, Y.-C. Wang, and M. W. Liemohn (2013), The importance of pickup oxygen ion precipitation to the Mars upper atmosphere under extreme solar wind conditions, *Geophys. Res. Lett.*, *40*, 1922–1927, doi:10.1002/grl.50415.
Feldman, P. D., et al. (2011), Rosetta-Alice observations of exospheric hydrogen and oxygen on Mars, *Icarus*, *214*, 394–399, doi:10.1016/j.icarus.2011.06.013.
Fite, W. L., R. F. Stebbings, D. G. Hummer, and R. T. Brackmann (1960), Ionization and charge transfer in proton-hydrogen atom collisions, *Phys. Rev.*, *119*(2), 663, doi:10.1103/PhysRev.119.663.
Fox, J. L., and A. B. Hać (2009), Photochemical escape of oxygen from Mars: A comparison of the exobase approximation to a Monte Carlo method, *Icarus*, *204*, 527–544, doi:10.1016/j.icarus.2009.07.005.
Fox, J. L., and A. B. Hać (2010), Isotope fractionation in the photochemical escape of O from Mars, *Icarus*, *208*(1), 176–191, doi:10.1016/j.icarus.2010.01.019.
Fox, J. L., and A. B. Hać (2014), The escape of O from Mars: Sensitivity to the elastic cross sections, *Icarus*, *228*, 375–385, doi:10.1016/j.icarus.2013.10.014.
Frahm, R. A., M. Yamauchi, J. D. Winningham, R. Lundin, J. R. Sharber, H. Nilsson, and A. J. Coates (2016), Foreshock ions observed behind the Martian bow shock, *Planet. Space Sci.*, *127*, 15–32, doi:10.1016/j.pss.2015.12.011.
Galli, A., et al. (2006), The hydrogen exospheric density profile measured with ASPERA-3/NPD, *Space Sci. Rev.*, *126*(1), 447–467, doi:10.1007/s11214-006-9089-7.
Goldstein, R., et al. (2015), The Rosetta Ion and Electron Sensor (IES) measurement of the development of pickup ions from comet 67P/Churyumov-Gerasimenko, *Geophys. Res. Lett.*, *42*, 3093–3099, doi:10.1002/2015GL063939.
Gronoff, G., et al. (2014), The precipitation of keV energetic oxygen ions at Mars and their effects during the comet Siding Spring approach, *Geophys. Res. Lett.*, *41*, 4844–4850, doi:10.1002/2014GL060902.
Halekas, J. S., et al. (2015a), The solar wind ion analyzer for MAVEN, *Space Sci. Rev.*, doi:10.1007/s11214-013-0029-z.
Halekas, J. S., et al. (2015b), MAVEN observations of solar wind hydrogen deposition in the atmosphere of Mars, *Geophys. Res. Lett.*, *42*, 8901–8909, doi:10.1002/2015GL064693.
Halekas, J. S., et al. (2017), Structure, dynamics, and seasonal variability of the mars-solar wind interaction: MAVEN solar wind ion analyzer inflight performance and science results, *J. Geophys. Res. Space Physics*, *122*, 547–578, doi:10.1002/2016JA023167.
Ip, W. H. (1988), On a hot oxygen corona of Mars, *Icarus*, *76*(1), 135–145, doi:10.1016/0019-1035(88)90146-7.
Ip, W. H. (1990), The fast atomic oxygen corona extent of Mars, *Geophys. Res. Lett.*, *17*(13), 2289–2292, doi:10.1029/GL017i013p02289.
Jain, S. K., et al. (2015), The structure and variability of Mars upper atmosphere as seen in MAVEN/IUVS dayglow observations, *Geophys. Res. Lett.*, *42*, 9023–9030, doi:10.1002/2015GL065419.
Jakosky, B. M., R. O. Pepin, R. E. Johnson, and J. L. Fox (1994), Mars atmospheric loss and isotopic fractionation by solar-wind-induced sputtering and photochemical escape, *Icarus*, *111*(2), 271–288, doi:10.1006/icar.1994.1145.
Jakosky, B. M., et al. (2015a), The Mars Atmosphere and Volatile Evolution (MAVEN) mission, *Space Sci. Rev.*, doi:10.1007/s11214-015-0139-x.
Jakosky, B. M., et al. (2015b), MAVEN observations of the response of Mars to an interplanetary coronal mass ejection, *Science*, *350*(6261), doi:10.1126/science.aad0210.
Jakosky, B. M., J. M. Grebowsky, J. G. Luhmann, and D. A. Brain (2015c), Initial results from the MAVEN mission to Mars, *Geophys. Res. Lett.*, *42*, 8791–8802, doi:10.1002/2015GL065271.
Jarvinen, R., and E. Kallio (2014), Energization of planetary pickup ions in the solar system, *J. Geophys. Res. Planets*, *119*, 219–236, doi:10.1002/2013JE004534.
Kallio, E., and H. Koskinen (1999), A test particle simulation of the motion of oxygen ions and solar wind protons near Mars, *J. Geophys. Res.*, *104*(A1), 557–579, doi:10.1029/1998JA900043.
Kaneda, K., N. Terada, and S. Machida (2009), Solar-wind control of the hot oxygen corona around Mars, *J. Geophys. Res.*, *114*, E02007, doi:10.1029/2008JE003234.
Kim, J., A. F. Nagy, J. L. Fox, and T. E. Cravens (1998), Solar cycle variability of hot oxygen atoms at Mars, *J. Geophys. Res.*, *103*(A12), 29,339–29,342, doi:10.1029/98JA02727.
Larson, D. E., et al. (2015), The MAVEN solar energetic particle investigation, *Space Sci. Rev.*, *195*(1–4), 153–172, doi:10.1007/s11214-015-0218-z.
Lee, C., et al. (2017), MAVEN observations of the solar cycle 24 space weather conditions at Mars, *J. Geophys. Res. Space Physics*, *122*, doi:10.1002/2016JA023495.

Lee, Y., M. R. Combi, V. Tenishev, S. W. Bougher, and R. J. Lillis (2015a), Hot oxygen corona at Mars and the photochemical escape of oxygen: Improved description of the thermosphere, ionosphere, and exosphere, *J. Geophys. Res. Planets*, *120*, 1880–1892, doi:10.1002/2015JE004890.

Lee, Y., M. R. Combi, V. Tenishev, S. W. Bougher, J. Deighan, N. M. Schneider, W. E. McClintock, and B. M. Jakosky (2015b), A comparison of 3-D model predictions of Mars' oxygen corona with early MAVEN IUVS observations, *Geophys. Res. Lett.*, *42*, 9015–9022, doi:10.1002/2015GL065291.

Lillis, R. J., et al. (2015), Characterizing atmospheric escape from Mars today and through time, with MAVEN, *Space Sci. Rev.*, *195*(1-4), 357–422, doi:10.1007/s11214-015-0165-8.

Lillis, R. J., C. O. Lee, D. Larson, J. G. Luhmann, J. S. Halekas, J. E. P. Connerney, and B. M. Jakosky (2016), Shadowing and anisotropy of solar energetic ions at Mars measured by MAVEN during the March 2015 solar storm, *J. Geophys. Res. Space Physics*, *121*, 2818–2829, doi:10.1002/2015JA022327.

Lillis, R. J., et al. (2017), Photochemical escape of oxygen from Mars: First results from MAVEN in situ data, *J. Geophys. Res. Space Physics*, *122*, doi:10.1002/2016JA023525.

Luhmann, J. G. (1990), A model of the ion wake of Mars, *Geophys. Res. Lett.*, *17*(6), 869–872, doi:10.1029/GL017i006p00869.

Luhmann, J. G., and J. U. Kozyra (1991), Dayside pickup oxygen ion precipitation at Venus and Mars: Spatial distributions, energy deposition and consequences, *J. Geophys. Res.*, *96*(A4), 5457–5467, doi:10.1029/90JA01753.

Luhmann, J. G., and K. Schwingenschuh (1990), A model of the energetic ion environment of Mars, *J. Geophys. Res.*, *95*(A2), 939–945, doi:10.1029/JA095iA02p00939.

Lundin, R., S. Barabash, M. Holmström, H. Nilsson, Y. Futaana, R. Ramstad, M. Yamauchi, E. Dubinin, and M. Fraenz (2013), Solar cycle effects on the ion escape from Mars, *Geophys. Res. Lett.*, *40*, 6028–6032, doi:10.1002/2013GL058154.

Ma, Y. J., et al. (2015), MHD model results of solar wind interaction with Mars and comparison with MAVEN plasma observations, *Geophys. Res. Lett.*, *42*, 9113–9120, doi:10.1002/2015GL065218.

Mahaffy, P. R., et al. (2015a), The neutral gas and ion mass spectrometer on the Mars Atmosphere and Volatile Evolution mission, *Space Sci. Rev.*, *195*, 49–73, doi:10.1007/s11214-014-0091-1.

Mahaffy, P. R., M. Benna, M. Elrod, R. V. Yelle, S. W. Bougher, S. W. Stone, and B. M. Jakosky (2015b), Structure and composition of the neutral upper atmosphere of Mars from the MAVEN NGIMS investigation, *Geophys. Res. Lett.*, *42*, doi:10.1002/2015GL065329.

Masunaga, K., K. Seki, D. A. Brain, X. Fang, Y. Dong, B. M. Jakosky, J. P. McFadden, J. S. Halekas, and J. E. P. Connerney (2016), O^+ ion beams reflected below the Martian bow shock: MAVEN observations, *J. Geophys. Res. Space Physics*, *121*, 3093–3107, doi:10.1002/2016JA022465.

Masunaga, K., et al. (2017), Statistical analysis of the reflection of incident O^+ pickup ions at Mars: MAVEN observations, *J. Geophys. Res. Space Physics*, *122*, doi:10.1002/2016JA023516.

McClintock, W. E., et al. (2015), The imaging ultraviolet spectrograph (IUVS) for the MAVEN mission, *Space Sci. Rev.*, *195*, 75–124, doi:10.1007/s11214-014-0098-7.

McFadden, J. P., et al. (2015), MAVEN SupraThermal and Thermal Ion Compostion (STATIC) instrument, *Space Sci. Rev.*, *195*, 199–256, doi:10.1007/s11214-015-0175-6.

Mitchell, D. L., et al. (2016), The MAVEN solar wind electron analyzer, *Space Sci. Rev.*, *200*, 495–528, doi:10.1007/s11214-015-0232-1.

Nagy, A. F., and T. E. Cravens (1988), Hot oxygen atoms in the upper atmospheres of Venus and Mars, *Geophys. Res. Lett.*, *15*(5), 433–435, doi:10.1029/GL015i005p00433.

Rahmati, A. (2016), Oxygen exosphere of Mars: Evidence from pickup ions measured by MAVEN, PhD dissertation, Department of Physics and Astronomy, Univ. of Kansas.

Rahmati, A., T. E. Cravens, A. F. Nagy, J. L. Fox, S. W. Bougher, R. J. Lillis, S. A. Ledvina, D. E. Larson, P. Dunn, and J. A. Croxell (2014), Pickup ion measurements by MAVEN: A diagnostic of photochemical oxygen escape from Mars, *Geophys. Res. Lett.*, *41*, 4812–4818, doi:10.1002/2014GL060289.

Rahmati, A., D. E. Larson, T. E. Cravens, R. J. Lillis, P. A. Dunn, J. S. Halekas, J. E. Connerney, F. G. Eparvier, E. M. B. Thiemann, and B. M. Jakosky (2015), MAVEN insights into oxygen pickup ions at Mars, *Geophys. Res. Lett.*, *42*, 8870–8876, doi:10.1002/2015GL065262.

Ramstad, R., S. Barabash, Y. Futaana, H. Nilsson, X.-D. Wang, and M. Holmström (2015), The Martian atmospheric ion escape rate dependence on solar wind and solar EUV conditions: 1. Seven years of Mars Express observations, *J. Geophys. Res. Planets*, *120*, 1298–1309, doi:10.1002/2015JE004816.

Romanelli, N., et al. (2016), Proton cyclotron waves occurrence rate upstream from Mars observed by MAVEN: Associated variability of the Martian upper atmosphere, *J. Geophys. Res. Space Physics*, *121*, 11,113–11,128, doi:10.1002/2016JA023270.

Sakai, S., A. Rahmati, D. L. Mitchell, T. E. Cravens, S. W. Bougher, C. Mazelle, W. K. Peterson, F. G. Eparvier, J. M. Fontenla, and B. M. Jakosky (2015), Model insights into energetic photoelectrons measured at Mars by MAVEN, *Geophys. Res. Lett.*, *42*, 8894–8900, doi:10.1002/2015GL065169.

Sakai, S., et al. (2016), Electron energetics in the Martian dayside ionosphere: Model comparisons with MAVEN data, *J. Geophys. Res. Space Physics*, *121*, 7049–7066, doi:10.1002/2016JA022782.

Stebbings, R. F., A. C. H. Smith, and H. Ehrhardt (1964), Charge transfer between oxygen atoms and O^+ and H^+ ions, *J. Geophys. Res.*, *69*(11), 2349–2355, doi:10.1029/JZ069i011p02349.

Thiemann, E. M. B., P. C. Chamberlin, F. G. Eparvier, T. N. Woods, S. W. Bougher, and B. M. Jakosky (2017), The MAVEN EUVM model of solar spectral irradiance variability at mars: Algorithms and results, *J. Geophys. Res. Space Physics*, *122*, doi:10.1002/2016JA023512.

Valeille, A., et al. (2009a), Three-dimensional study of Mars upper thermosphere/ionosphere and hot oxygen corona: 1. General description and results at equinox for solar low conditions, *J. Geophys. Res.*, *114*, E11005, doi:10.1029/2009JE003388.

Valeille, A., et al. (2009b), Three-dimensional study of Mars upper thermosphere/ionosphere and hot oxygen corona: 2. Solar cycle, seasonal variations and evolution over history, *J. Geophys. Res.*, *114*, E11006, doi:10.1029/2009JE003389.

Valeille, A., M. R. Combi, V. Tenishev, S. W. Bougher, and A. F. Nagy (2010), A study of suprathermal oxygen atoms in Mars upper thermosphere and exosphere over the range of limiting conditions, *Icarus*, *206*(1), 18–27, doi:10.1016/j.icarus.2008.08.018.

Wang, Y.-C., J. G. Luhmann, X. Fang, F. Leblanc, R. E. Johnson, Y. Ma, and W.-H. Ip (2015), Statistical studies on Mars atmospheric sputtering by precipitating pickup O^+: Preparation for the MAVEN mission, *J. Geophys. Res. Planets*, *120*, 34–50, doi:10.1002/2014JE004660.

Wang, Y.-C., J. G. Luhmann, A. Rahmati, F. Leblanc, R. E. Johnson, T. E. Cravens, and W.-H. Ip (2016), Cometary sputtering of the Martian atmosphere during the Siding Spring encounter, *Icarus*, *272*, 301–308, doi:10.1016/j.icarus.2016.02.040.

Yagi, M., F. Leblanc, J. Y. Chaufray, F. Gonzalez-Galindo, S. Hess, and R. Modolo (2012), Mars exospheric thermal and non-thermal components: Seasonal and local variations, *Icarus*, *221*(2), 682–693, doi:10.1016/j.icarus.2012.07.022.

Yamauchi, M., Y. Futaana, A. Fedorov, R. A. Frahm, E. Dubinin, R. Lundin, J.-A. Sauvaud, J. D. Winningham, S. Barabash, and M. Holmstrom (2012), Ion acceleration by multiple reflections at Martian bow shock, *Earth Planets Space*, *64*(2), 61–71, doi:10.5047/eps.2011.07.007.

Yamauchi, M., R. Lundin, R. A. Frahm, J.-A. Sauvaud, M. Holmström, and S. Barabash (2015a), Oxygen foreshock of Mars, *Planet. Space Sci.*, *119*, 48–53, doi:10.1016/j.pss.2015.08.003.

Yamauchi, M., et al. (2015b), Seasonal variation of Martian pick-up ions: Evidence of breathing exosphere, *Planet. Space Sci.*, *119*, 54–61, doi:10.1016/j.pss.2015.09.013.